

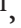



Regulation of body weight and energy homeostasis by neuronal cell adhesion molecule 1

Thomas Rathjen^{1,17}, Xin Yan^{1,17}, Natalia L Kononenko²⁻⁴, Min-Chi Ku^{1,5} , Kun Song¹, Leiron Ferrarese^{1,4}, Valentina Tarallo⁶, Dmytro Puchkov², Gaga Kochlamazashvili², Sebastian Brachs⁷, Luis Varela⁸, Klara Szigeti-Buck⁸, Chun-Xia Yi⁹, Sonja C Schriever⁹ , Sudhir Gopal Tattikota¹, Anne Sophie Carlo¹, Mirko Moroni¹, Jan Siemens¹⁰, Arnd Heuser¹, Louise van der Weyden¹¹, Andreas L Birkenfeld^{12,13} , Thoralf Niendorf^{1,5,14}, James F A Poulet^{1,4}, Tamas L Horvath^{8,15}, Matthias H Tschöp⁹, Matthias Heinig¹⁶, Mirko Trajkovski⁶, Volker Haucke^{2,4} & Matthew N Poy¹ 

Susceptibility to obesity is linked to genes regulating neurotransmission, pancreatic beta-cell function and energy homeostasis. Genome-wide association studies have identified associations between body mass index and two loci near *cell adhesion molecule 1 (CADM1)* and *cell adhesion molecule 2 (CADM2)*, which encode membrane proteins that mediate synaptic assembly. We found that these respective risk variants associate with increased *CADM1* and *CADM2* expression in the hypothalamus of human subjects. Expression of both genes was elevated in obese mice, and induction of *Cadm1* in excitatory neurons facilitated weight gain while exacerbating energy expenditure. Loss of *Cadm1* protected mice from obesity, and tract-tracing analysis revealed *Cadm1*-positive innervation of POMC neurons via afferent projections originating from beyond the arcuate nucleus. Reducing *Cadm1* expression in the hypothalamus and hippocampus promoted a negative energy balance and weight loss. These data identify essential roles for *Cadm1*-mediated neuronal input in weight regulation and provide insight into the central pathways contributing to human obesity.

Obesity is one of the leading global health threats, with a projected burden on public health that appears to be interminable¹. Numerous reports support a crucial role for genetic susceptibility to the risk for obesity and related metabolic disorders, including type 2 diabetes²⁻⁴. Recent studies have identified ~100 susceptibility loci, which associate with body mass index and map near genes that are known to function in the CNS⁵⁻⁷. Among the genes identified in these studies are *CADM1* and *CADM2* (also known as *SYNCAM1* and *SYNCAM2*, respectively)⁷, which encode two immunoglobulin-domain-containing adhesion proteins that mediate synaptic assembly in the CNS⁸⁻¹⁰. Here we illustrate how increased expression of both *Cadm1* and *Cadm2* in regions of the brain facilitates weight gain and how targeting their expression can provide new insight into the mechanisms leading to human obesity.

RESULTS

SNPs associate with increased *CADM* genes

Recent genome-wide association studies identified two single-nucleotide polymorphisms (SNPs), rs12286929 and rs13078807, in proximity

to *CADM1* and *CADM2*, respectively, which associate with increased body mass index (BMI) in human subjects^{6,7}. The SNP rs12286929 is located in an intergenic region 17 kb downstream of the 3' end of *CADM1* and the SNP rs13078807 is located in the second intron of *CADM2*. We analyzed expression quantitative trait locus (eQTL) data from ten distinct regions of the brain available from the Genotype-Tissue Expression (GTEx) consortium and observed that both risk alleles (the alleles associated with increased BMI) were associated with increased mRNA expression of their proximal genes in the hypothalamus and cerebellum of human subjects (*CADM1*: hypothalamus, allelic effect = 10% s.d., $P = 0.05$; cerebellum, allelic effect = 17% s.d., $P = 0.02$; *CADM2*: hypothalamus, allelic effect = 19% s.d., $P = 0.05$; cerebellum, allelic effect = 30% s.d., $P = 0.004$; **Fig. 1a,b** and **Supplementary Fig. 1a,b**)¹¹. *Cadm1* and *Cadm2* have been shown to interact via their extracellular domains (**Supplementary Fig. 2a**)^{9,12} and might therefore act synergistically. Thus, we evaluated how altered expression of these genes contributes to the regulation of body weight using rodent models.

¹Max Delbrück Center for Molecular Medicine, Berlin, Germany. ²Leibniz Institute for Molecular Pharmacology, Berlin, Germany. ³CECAD Research Center, University of Cologne, Cologne, Germany. ⁴Cluster of Excellence NeuroCure, Neuroscience Research Center, Charité-Universitätsmedizin Berlin, Berlin, Germany. ⁵Berlin Ultrahigh Field Facility (B.U.F.F.), Max Delbrück Center for Molecular Medicine, Berlin, Germany. ⁶University of Geneva, Medical Faculty, Department of Cell Physiology and Metabolism, Centre Médical Universitaire (CMU), Geneva, Switzerland. ⁷Charité - Universitätsmedizin Berlin, Department of Endocrinology, Diabetes and Nutrition, Center for Cardiovascular Research, Berlin, Germany. ⁸Program in Integrative Cell Signaling and Neurobiology of Metabolism, Department of Comparative Medicine, Yale University School of Medicine, New Haven, Connecticut, USA. ⁹Institute for Diabetes and Obesity, Helmholtz Centre for Health and Environment and Division of Metabolic Diseases, Technical University Munich, Munich, Germany. ¹⁰Department of Pharmacology, University of Heidelberg, Heidelberg, Germany. ¹¹Wellcome Trust Sanger Institute, Wellcome Trust Genome Campus, Hinxton, Cambridge, UK. ¹²Section of Metabolic Vascular Medicine and Paul Langerhans Institute Dresden of the Helmholtz Center Munich at University Hospital and Faculty of Medicine, TU Dresden, Medical Clinic III, University Clinic Dresden, Dresden, Germany. ¹³Division of Diabetes and Nutritional Sciences, Faculty of Life Sciences and Medicine, King's College London, London, UK. ¹⁴Experimental and Clinical Research Center, Max Delbrück Center for Molecular Medicine, Berlin, Germany. ¹⁵Department of Anatomy and Histology, University of Veterinary Sciences, Budapest, Hungary. ¹⁶Helmholtz Zentrum München, Institute of Computational Biology, Neuherberg, Germany. ¹⁷These authors contributed equally to this work. Correspondence should be addressed to M.N.P. (matthew.poy@mdc-berlin.de).

Received 6 April; accepted 24 May; published online 19 June 2017; doi:10.1038/nn.4590

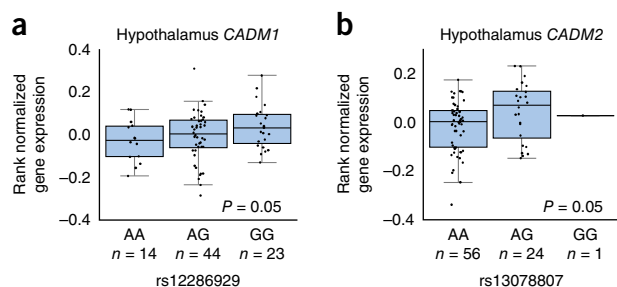


Figure 1 BMI risk SNPs associate with increased *CADM1* and *CADM2* expression in the hypothalamus of human subjects. **(a)** Elevated expression of *CADM1* associates with risk allele (G) of rs12286929 in hypothalamus. **(b)** Genotype-dependent expression levels of *CADM2* for the SNP rs13078807. The risk allele (G) is associated with higher expression levels in human hypothalamus. Statistical analyses are described in the Online Methods and **Supplementary Table 3**. Boxplots show the 25% and 75% quantiles of normalized mRNA expression levels (y axis), solid horizontal lines indicate the median, and whiskers indicate the 10% and 90% quantiles.

Consistent with our eQTL analysis, we observed increased *Cadm1* and *Cadm2* protein levels in isolated synaptosomes from hypothalamus, cerebellum, and hippocampus of obese and insulin-resistant *Lep^{ob/ob}* mice compared with lean littermate controls (**Fig. 2a** and **Supplementary Fig. 2b,c**). Given that administration of a low-carbohydrate, ketogenic diet has been shown to improve insulin sensitivity and random blood glucose levels in *Lep^{ob/ob}* animals¹³, we tested its effect on neuronal *Cadm1* expression. Feeding 16-week-old *Lep^{ob/ob}* animals this diet for 60 d reduced the expression of *Cadm1* in the hippocampus and cerebellar regions, whereas the diet elicited no change in wild-type (WT) mice (**Supplementary Fig. 2d–g**).

These results indicate that increased neuronal expression of *Cadm1* and *Cadm2* in the human and mouse brain associates with elevated body weight and indicate that these two genes may be important for maintaining energy balance. The reduction of *Cadm1* expression in multiple brain regions of *Lep^{ob/ob}* mice on a ketogenic diet also underscores the highly regulated nature of *Cadm1* and suggests that it may contribute to adaptive or homeostatic plasticity in neuronal networks in accordance with nutrient state.

Cadm1 regulates energy homeostasis

To understand the endogenous function of *Cadm1*, we first characterized a global loss-of-function mouse model (*Cadm1*KO) and observed a reduction in body weight compared with littermate controls starting at postnatal day 3 (**Fig. 2b–d** and **Supplementary Fig. 3a**). A concomitant decrease in *Cadm2* expression independent of changes on its mRNA level indicates that *Cadm1* may contribute to the stability of *Cadm2* and its function (**Fig. 2c**), consistent with their physical association. *Cadm1*KO mice had a lower proportion of body fat than controls, but showed indistinguishable random glucose and insulin levels (**Supplementary Tables 1** and **2**). Body length was slightly lower in *Cadm1*KO mice (9.1 ± 0.1 WT versus 8.5 ± 0.1 cm *Cadm1*KO mice, $P < 0.05$ at age 12 weeks), as was the body weight to length ratio, suggesting that the decrease in body mass was a result of both reduced growth rate and adipose mass (**Supplementary Fig. 3b** and **Supplementary Table 2**). We performed insulin, glucose and pyruvate tolerance tests (ITT, GTT and PTT, respectively) and observed lower glucose levels in *Cadm1*KO mice than in controls suggesting systemic insulin sensitivity was improved (**Supplementary Fig. 3c–e**). We next tested sensitivity to leptin, another potent regulator of energy

homeostasis. Intraperitoneal administration of leptin resulted in a greater decrease of both body mass and food intake in *Cadm1*KO mice (**Supplementary Fig. 3f,g**). Moreover, consistent with improved sensitivity to leptin, basal plasma leptin levels were significantly lower ($P = 0.0245$) and plasma adiponectin levels were elevated in mutant animals compared with controls ($P = 0.0305$) (**Supplementary Table 1**).

As insulin and leptin signaling in the brain both influence body mass and energy homeostasis^{14–16}, we next addressed whether energy expenditure rates were altered in *Cadm1*KO animals. O_2 consumption, CO_2 production, energy expenditure and locomotor activity were all higher in *Cadm1*KO mice, whereas food intake, core body temperature and nutrient partitioning (on the basis of respiratory exchange rate, RER) were normal (**Supplementary Fig. 3h–k**). Evaluation of energy expenditure using analysis of covariance (ANCOVA), as plotted in relation to lean body mass, confirmed the increased rates in *Cadm1*KO animals (**Fig. 2e**)¹⁷. When energy expenditure was plotted in relation to locomotor activity, this comparison confirmed that *Cadm1*KO animals maintain increased energy expenditure and that this elevated rate was directly correlated to increased activity (**Supplementary Fig. 3l,m**). Similar to *Cadm1*KO mice, global deletion of *Cadm2* in mice (*Cadm2*KO) also resulted in lower body weight, as well as increased insulin sensitivity, glucose tolerance and energy expenditure without any change in food intake; further suggesting that *Cadm1* and *Cadm2* may interact to coordinately contribute to body weight regulation (**Supplementary Fig. 3n–y** and **Supplementary Table 2**).

Pro-opiomelanocortin (POMC)-expressing neurons are among the most studied cells in the brain as a result of their regulatory role in glucose utilization and energy expenditure^{18,19}. In WT C57BL/6 mice, we observed that ~12% of POMC-expressing neurons expressed *Cadm1*, as determined by immunostaining (**Supplementary Fig. 4a,b**). We found no changes in the expression of the hypothalamic neuropeptides *Pomc*, *Npy* and *Agrp* in *Cadm1*KO mice in contrast with *Lep^{ob/ob}* controls (**Supplementary Fig. 4c**). Given that several studies have now reported on *Cadm1* function in neuronal signaling and plasticity^{20,21}, we sought to determine whether the POMC neurons in the arcuate nucleus (ARC) were functionally altered in *Cadm1*KO mice, and we first analyzed miniature excitatory and inhibitory postsynaptic currents (EPSCs and IPSCs, respectively). Recordings of IPSCs in POMC neurons from *Cadm1*KO mice showed a substantial reduction in IPSC frequency without any effect on mean amplitude in comparison with littermate controls, whereas no difference was observed in EPSCs derived from their glutamatergic inputs (**Supplementary Fig. 4d,e**). We then quantified the number of synapses in contact with these neurons. Loss of *Cadm1* resulted in a significant increase in the number of asymmetric excitatory synapses (2.3 ± 0.5 in WT and 7.1 ± 0.9 synapses in *Cadm1*KO, $P < 0.001$) at POMC neurons (**Supplementary Fig. 4f–h**), which is distinct from the very mild reduction of excitatory synapse number in hippocampal CA1 neurons that has been reported²⁰. The increase in excitatory contacts at POMC neurons in *Cadm1*KO mice and the absence of any change in mEPSCs frequency in these neurons may indicate that many of the observed excess connections are ‘silent’ and thereby yield an increased capacity for synaptic plasticity²². Homeostatic changes in synaptic plasticity and/or the imbalance of excitation and inhibition in the brain^{20,23} may conceivably underlie the effects on energy homeostasis in *Cadm1*KO mice.

Induction of *Cadm1* promotes weight gain

To date, the contribution of *Cadm1* and *Cadm2* in both glutamatergic and GABAergic populations to energy homeostasis has not

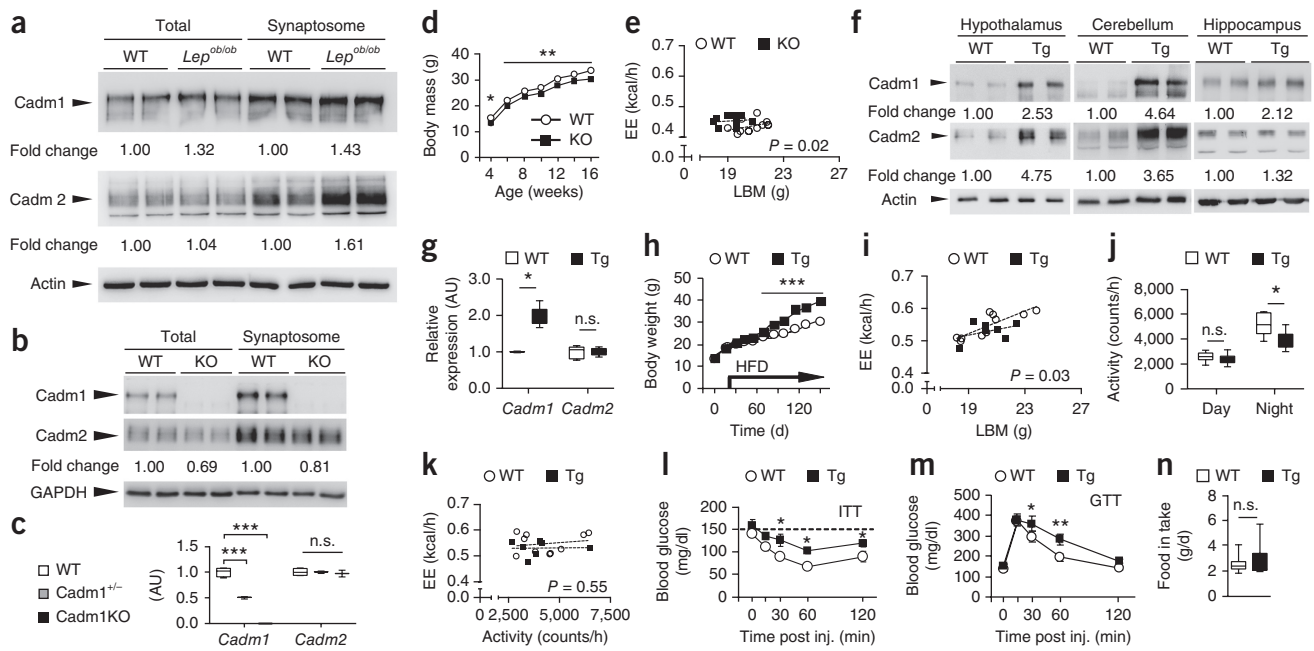


Figure 2 Induction of *Cadm1* in excitatory neurons increases body weight. (a) Western blot analysis of *Cadm1* and *Cadm2* in total and synaptosome-enriched lysates from the hypothalamus of 4-week-old *Lep^{ob/ob}* mice and littermate controls. (b) Western blot analysis of *Cadm1* and *Cadm2* in total and synaptosome-enriched lysates from the hippocampus of 3-week-old *Cadm1*KO and control littermates. (c) Quantitative reverse-transcription PCR analysis of *Cadm1* and *Cadm2* expression in hippocampus of 5-week-old *Cadm1*KO mice, *Cadm1*^{+/-} (heterozygous) and control littermates (WT) ($n = 3-4$). (d) Body weight curves of *Cadm1*KO mice ($n = 10$) and littermate controls ($n = 10$). (e) Energy expenditure (EE) of individual animals plotted against lean body mass (LBM) in 12-week-old *Cadm1*KO ($n = 9$) and littermate controls ($n = 10$). (f) Western blot analysis of *Cadm1* and *Cadm2* in total lysates from hypothalamus, cerebellum and hippocampus of 14-week-old Tg-*Cadm1* mice and control littermates. (g) Quantification of *Cadm1* and *Cadm2* expression from cultured primary hippocampal neurons from Tg-*Cadm1* mice ($n = 5$) and wild-type littermate controls ($n = 5$) after 5 d of treatment with doxycycline. (h) Body weight curves of Tg-*Cadm1* mice ($n = 5$) and littermate controls ($n = 8$) following doxycycline treatment at 4 weeks of age. High-fat-diet feeding was initiated on day 25 of doxycycline treatment. (i) Energy expenditure of individual animals plotted against LBM in 16-week-old Tg-*Cadm1* mice ($n = 7$) and littermate controls ($n = 10$). (j) Quantification of locomotor activity measured in 16-week-old Tg-*Cadm1* mice ($n = 7$) and controls ($n = 8$). (k) Energy expenditure of individual animals plotted against locomotor activity in 16-week-old Tg-*Cadm1* mice ($n = 7$) and littermate controls ($n = 10$). (l) Blood glucose measurements during an ITT on 20-week-old Tg-*Cadm1* mice ($n = 5$) and control littermates ($n = 6$). (m) Glucose measurements during a GTT on 18-week-old Tg-*Cadm1* mice ($n = 5$) and littermates ($n = 7$). (n) Quantification of food intake in 16-week-old Tg-*Cadm1* mice ($n = 7$) and littermates ($n = 8$). All results in **d**, **h**, **l** and **m** are presented as mean \pm s.e.m. * $P < 0.05$, ** $P < 0.01$, *** $P < 0.001$. Boxplots show median, lower and upper quartiles (box), and minimum and maximum (whiskers). Statistical analyses are described in the Online Methods and **Supplementary Table 3**.

been directly addressed (**Supplementary Fig. 5a-e**). Previous studies have shown that *Cadm1*'s role in synaptic plasticity and the balance of network excitability is derived from its expression in excitatory neurons^{20,21}. On the basis of these results, we directly tested whether increasing *Cadm1* expression in a subset of glutamatergic neurons would contribute to energy homeostasis by generating a mouse line bearing a transgene encoding *Cadm1* under the control of seven tandem doxycycline-responsive elements (Tg-*Cadm1* mice; **Fig. 2f** and **Supplementary Fig. 5f**). These mice also expressed Cre recombinase under the control of the *Slc17a6* promoter, which leads to vesicular glutamate transporter 2 expression, and lox-rtTA (where the reverse tetracycline transactivator is expressed in the presence of Cre recombinase), and treatment of doxycycline via drinking water resulted in overexpression of *Cadm1* in many brain regions, including a $\sim 2-3$ -fold increase in the hypothalamus (**Fig. 2f,g**). Tg-*Cadm1* mice exhibited increased body weight and adipose mass ~ 30 d after initiation of high-fat-diet feeding compared with controls (**Fig. 2h** and **Supplementary Table 2**). The induction of *Cadm1* expression in *Vglut2*-expressing excitatory neurons reduced energy expenditure and locomotor activity and attenuated insulin sensitivity and glucose tolerance, further suggesting that the higher *Cadm1* levels observed in *Lep^{ob/ob}* mice contributed to the obesity, insulin resistance and

hyperglycemia (**Fig. 2i-m** and **Supplementary Fig. 5f,g**). Increasing *Cadm1* levels promoted both *Cadm2* expression and their colocalization, without having any effect on *Cadm2* mRNA levels, providing further evidence that the stability of *Cadm2* is dependent on *Cadm1* expression (**Fig. 2g** and **Supplementary Fig. 5h-j**). As observed in *Cadm1*KO and *Cadm2*KO mice, the effect on body weight in Tg-*Cadm1* mice was associated with an alteration in energy expenditure and not in food intake (**Fig. 2n**).

To further distinguish the function of *Cadm1* in specific neuronal populations, we next eliminated its expression in either *Vglut2*-expressing excitatory or *Vgat*-expressing inhibitory neurons by crossing *Slc17a6-Cre* (also known as *VGLUT2-Cre*) and vesicular GABA transporter (*Slc32a1*)-*Cre* mouse lines with a *Cadm1* conditional allele (*Slc17a6-Cre, Cadm1^{fllox/fllox}* and *Slc32a1-Cre, Cadm1^{fllox/fllox}*, respectively; **Supplementary Fig. 6a-d**)¹⁹. Similar to *Cadm1*KO animals, *Slc17a6-Cre, Cadm1^{fllox/fllox}* mice recapitulated the effects on body mass, insulin and pyruvate challenge, energy expenditure, and activity (**Fig. 3a-f**, **Supplementary Fig. 6e,f**, and **Supplementary Table 2**). Infrared image analysis revealed that *Slc17a6-Cre, Cadm1^{fllox/fllox}* mice exhibited elevated body temperatures in the eye, inguinal subcutaneous adipose tissue (iSAT) and interscapular brown adipose tissue (BAT) regions after exposure to cold without an effect on food

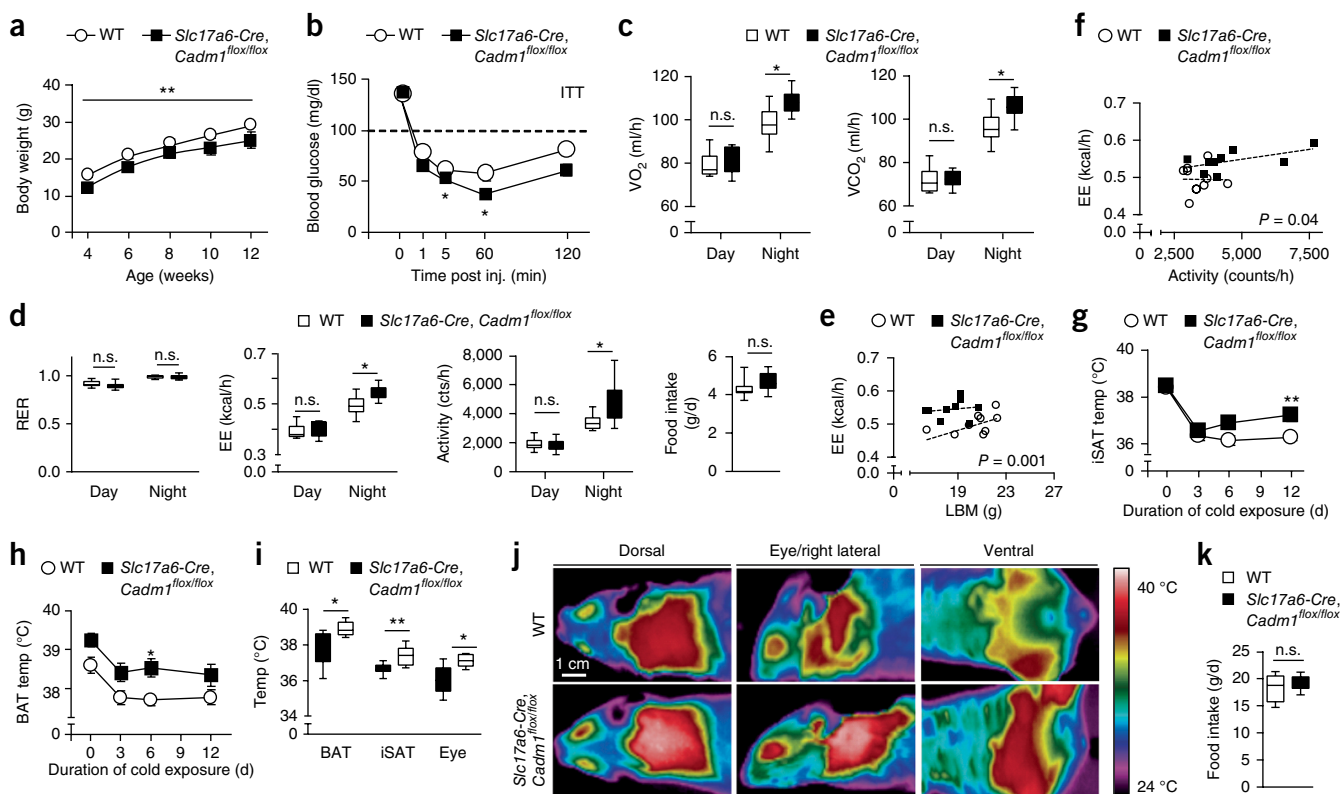


Figure 3 Loss of *Cadm1* in excitatory neurons affects body weight, energy homeostasis and thermogenesis. (a) Body weight curves of *Slc17a6-Cre, Cadm1^{flox/flox}* mice ($n = 12$) and littermate controls ($n = 14$) from 4–12 weeks of age. (b) Glucose measurements during an ITT on 12-week-old *Slc17a6-Cre, Cadm1^{flox/flox}* mice ($n = 5$) and control littermates ($n = 6$). (c,d) Quantification of O_2 consumption, CO_2 production, RER, energy expenditure (EE), locomotor activity and food intake in 12-week-old *Slc17a6-Cre, Cadm1^{flox/flox}* mice ($n = 9$) and littermate controls ($n = 10$). (e) Energy expenditure of individual animals plotted against lean body mass from 12-week-old *Slc17a6-Cre, Cadm1^{flox/flox}* mice ($n = 9$) and littermate controls ($n = 10$). (f) Energy expenditure of individual animals plotted against locomotor activity in 12-week-old *Slc17a6-Cre, Cadm1^{flox/flox}* mice ($n = 9$) and littermate controls ($n = 10$). (g) iSAT temperature measurements from 12-week-old *Slc17a6-Cre, Cadm1^{flox/flox}* mice ($n = 5$) and control littermates ($n = 8$) during cold challenge. (h) BAT temperature measurements from 12-week-old *Slc17a6-Cre, Cadm1^{flox/flox}* mice ($n = 5$) and control littermates ($n = 8$) during cold challenge. (i) Temperature measurements of BAT, iSAT and eye regions from 12-week-old *Slc17a6-Cre, Cadm1^{flox/flox}* mice ($n = 5$) and control littermates ($n = 8$) after 1 week of exposure to cold. (j) Representative near-infrared analysis of 12-week-old *Slc17a6-Cre, Cadm1^{flox/flox}* mice and control littermates after 1 week of cold exposure. (k) Quantification of daily food intake of *Slc17a6-Cre, Cadm1^{flox/flox}* mice ($n = 5$) and control littermates ($n = 8$) after cold exposure. All results in **a**, **b**, **g** and **h** are presented as mean \pm s.e.m. * $P < 0.05$, ** $P < 0.01$. Boxplots show median, lower and upper quartiles (box), and minimum and maximum (whiskers). Statistical analyses are described in the Online Methods and **Supplementary Table 3**.

intake (**Fig. 3g–k**). In comparison with *Slc17a6-Cre, Cadm1^{flox/flox}* mice, loss of *Cadm1* in *Slc32a1-Cre* neurons resulted only in reduced insulin sensitivity compared with controls (**Supplementary Fig. 6g–i**). No changes were observed in body weight, glucose tolerance, energy expenditure or food intake, indicating that the effect of altered *Cadm1* expression on body weight and energy homeostasis appears to be derived from its expression in *Vglut2*-expressing excitatory neurons.

Reduction of *Cadm1* protects from obesity

Underscoring the functional importance of *Cadm1* in excitatory neurons, *Slc17a6-Cre, Cadm1^{flox/flox}* mice were protected from diet-induced obesity and insulin resistance after challenging these mice with a high-fat regimen (**Fig. 4a–d**). To accurately assess the effect of *Cadm1* on systemic insulin sensitivity and tissue-specific glucose turnover rates in response to this diet, we performed hyperinsulinemic-euglycemic clamp studies on *Slc17a6-Cre, Cadm1^{flox/flox}* animals after 8 weeks of feeding. Basal blood glucose and insulin levels did not differ with *Cadm1* status; however, after clamping glucose levels at 120 mg dl^{-1} , we found that the glucose infusion rate was significantly

elevated ($P = 0.0291$) in *Slc17a6-Cre, Cadm1^{flox/flox}* animals, confirming improved overall insulin sensitivity (**Supplementary Fig. 6m,n**). Although basal hepatic glucose output was unchanged, clamped hepatic output was significantly decreased (**Supplementary Fig. 6o**). In addition, consistent with improved hepatic insulin sensitivity, no differences were observed in hepatic glucose uptake, rate of glycolysis or glycogen synthesis, or insulin levels at the end of the clamp between *Slc17a6-Cre, Cadm1^{flox/flox}* and WT animals (**Supplementary Fig. 6p**). The ability to reverse obesity and improve glucose homeostasis after targeting neuronal *Cadm1* expression was further shown after we crossed *Slc17a6-Cre, Cadm1^{flox/flox}* mice onto the *Lep^{ob/ob}* background (*ob/MUT*) and observed lower body mass, circulating random glucose and plasma insulin levels compared with *Lep^{ob/ob}* littermates (**Fig. 4e–g**, and **Supplementary Table 2**). Results from an ITT, as well as energy expenditure and liver gene expression analysis, also showed that *ob/MUT* mice were more insulin sensitive and the increased beta-cell mass symptomatic of an insulin-resistant state was significantly reversed in comparison with *Lep^{ob/ob}* controls (**Fig. 4h–k**). Although *Lep^{ob/ob}* mice exhibited several metabolic alterations beyond weight gain and hyperglycemia, these results further illustrate the fact that

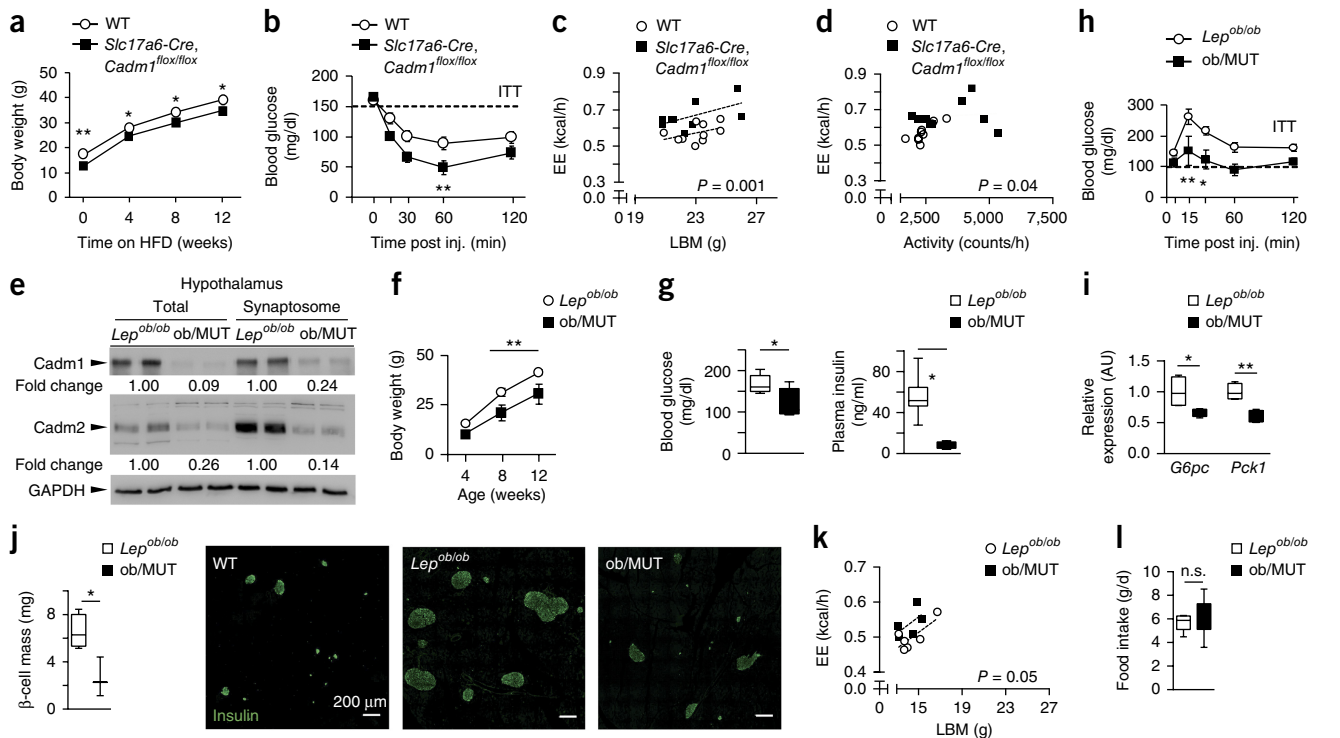


Figure 4 Loss of neuronal *Cadm1* protects from genetically and diet-induced obesity and insulin resistance. (a) Body weight curves of *Slc17a6-Cre, Cadm1^{fllox/fllox}* mice ($n = 10$) and littermate controls ($n = 6$) on high fat diet (HFD). (b) Glucose measurements during an ITT from 16-week-old *Slc17a6-Cre, Cadm1^{fllox/fllox}* mice ($n = 7$) and control littermates ($n = 10$) after 10 weeks on HFD. (c) Energy expenditure (EE) from individual animals plotted against lean body mass in 16-week-old *Slc17a6-Cre, Cadm1^{fllox/fllox}* mice ($n = 9$) and littermate controls ($n = 10$) after 10 weeks on HFD. (d) Energy expenditure from individual animals plotted against locomotor activity in 16-week-old *Slc17a6-Cre, Cadm1^{fllox/fllox}* mice ($n = 9$) and littermate controls ($n = 10$) after 10 weeks on HFD. (e) Western blot analysis of *Cadm1* and *Cadm2* in total and synaptosome-enriched lysates from hypothalamus of 12-week-old *Slc17a6-Cre, Cadm1^{fllox/fllox}* crossed onto the *Lep^{ob/ob}* background (*ob/MUT*) mice and *Lep^{ob/ob}* littermates. (f) Body weight curves of *ob/MUT* mice ($n = 5$) and *Lep^{ob/ob}* littermate controls ($n = 9$) from 4–12 weeks of age. (g) Random glucose and plasma insulin measurements in *ob/MUT* mice ($n = 4$) and *Lep^{ob/ob}* littermate controls ($n = 8$). (h) Glucose measurements during an ITT on 12-week-old *ob/MUT* mice ($n = 5$) and control *Lep^{ob/ob}* littermates ($n = 9$). (i) Quantitative reverse-transcription PCR analysis of *G6pc* and *Pck1* expression in liver of 12-week-old *ob/MUT* mice ($n = 4$) and control *Lep^{ob/ob}* littermates ($n = 4$). (j) Quantification of pancreatic beta-cell mass in *ob/MUT* mice ($n = 3$) and littermate *Lep^{ob/ob}* controls ($n = 4$) from 12 weeks of age. Immunohistochemistry of representative pancreatic sections from WT, *Lep^{ob/ob}* and *ob/MUT* mice after detection of insulin (green). (k) Energy expenditure from individual animals plotted against lean body mass in 12-week-old *ob/MUT* mice ($n = 5$) and *Lep^{ob/ob}* littermates ($n = 6$). (l) Quantification of food intake measured in 12-week-old *ob/MUT* mice ($n = 5$) and littermate *Lep^{ob/ob}* controls ($n = 6$). All results in a, b, h and f are presented as mean \pm s.e.m. * $P < 0.05$, ** $P < 0.01$. Boxplots show median, lower and upper quartiles (box), and minimum and maximum (whiskers). Statistical analyses are described in the Online Methods and **Supplementary Table 3**.

the loss of *Cadm1* in excitatory neurons protected mice from both genetically and diet-induced obesity and insulin resistance by improving energy expenditure, glucose homeostasis and insulin sensitivity independently of any change in food intake (Fig. 4l). Notably, these observations establish *Cadm1* as a potential target in the brain for therapeutic intervention in alleviating the complications associated with diabetes and obesity.

Cadm1 functions in multiple neuronal circuits

Cadm1 is present throughout the brain and has been shown to regulate synapse formation, morphology, plasticity and network excitability^{20,21,24}. The broad expression pattern of *Slc17a6-Cre* suggests that *Cadm1* may contribute to energy homeostasis via multiple brain regions. To elucidate the circuits that contribute to *Cadm1* function in systemic energy homeostasis, we analyzed the effects of *Cadm1* loss in *Vglut2⁺* excitatory neurons on hippocampal synapse number and function. In spite of its described role in hippocampal synapse formation during the postnatal period, synapse numbers in this region were unchanged in adult *Slc17a6-Cre, Cadm1^{fllox/fllox}* mice compared with

littermate controls (Supplementary Fig. 7a,b)²⁰. Postsynaptic density length and postsynaptic density protein 95 (PSD-95) expression were decreased in the hippocampus of *Slc17a6-Cre, Cadm1^{fllox/fllox}* animals, suggesting that *Cadm1* function may vary with age, cellular context or metabolic state (Supplementary Fig. 7c,d). Electrophysiologic analysis revealed increased basal synaptic transmission, supporting recent observations of *Cadm1* in synaptic transmission by balancing excitatory and inhibitory transmission (Supplementary Fig. 7e)²¹. In addition, we observed increased long-term depression and long-term potentiation, supporting previous observations on the role of *Cadm1* in synaptic plasticity (Supplementary Fig. 7f,g)²⁰ and on the promotion of hippocampal plasticity by locomotor activity in rodents^{25,26}. These observations suggest that *Cadm1* regulates energy and glucose homeostasis by modulating excitatory synapse function in the hippocampus.

To directly address the role of *Cadm1* in the regulation of body weight and energy homeostasis in hippocampal excitatory neurons, we specifically eliminated its expression in this brain region via stereotaxic injection of a Cre-recombinase-expressing adeno-associated virus (rAAV8/CamKII-mCherry-Cre) (Fig. 5a,b). The AAV coexpressed

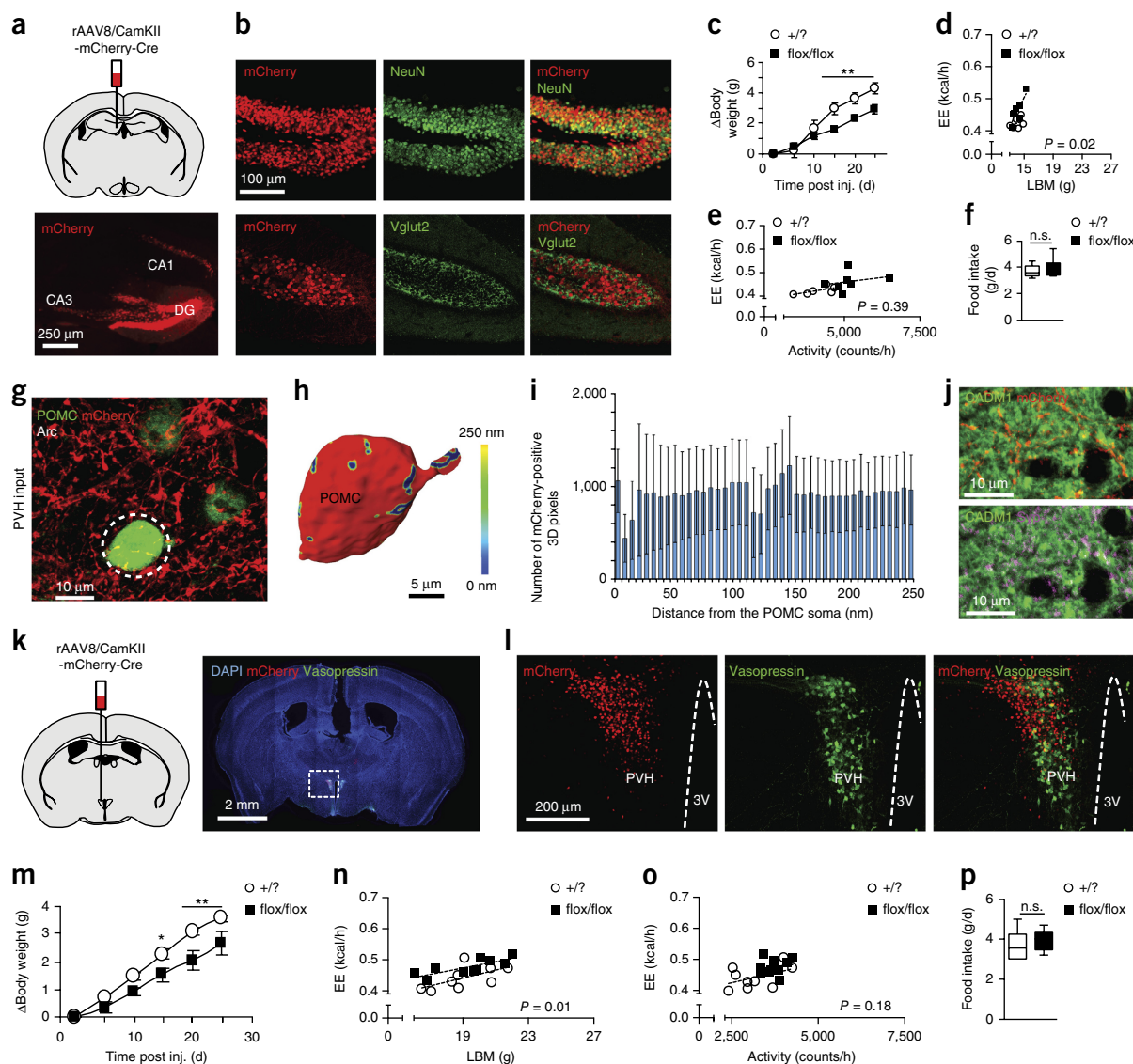


Figure 5 Targeting *Cadm1* expression in the hippocampus and hypothalamus reduces body weight. (a) Representative coronal brain section of *Cadm1^{flx/flx}* mice after stereotaxic rAAV8-CaMKIIa-mCherry-Cre (AAV-Cre) injection in the dentate gyrus (DG) and CA3 regions to target *Cadm1* expression in hippocampal neurons. (b) Colocalization of mCherry with NeuN and Vglut2 after delivery of AAV-CaMKIIa-Cre to the hippocampus. (c) Body weight curves of *Cadm1^{flx/flx}* mice ($n = 6$) and control littermates (+/?) ($n = 6$) after delivery of AAV-Cre to the hippocampus. (d) Energy expenditure (EE) from individual animals plotted against lean body mass in 9-week-old *Cadm1^{flx/flx}* mice ($n = 7$) and control littermates (+/?) ($n = 6$) after delivery of AAV-Cre to the hippocampus. (e) Energy expenditure from individual animals plotted against activity measured in 9-week-old *Cadm1^{flx/flx}* mice ($n = 7$) and control littermates (+/?) ($n = 6$) after delivery of AAV-Cre to the hippocampus. (f) Quantification of food intake measured in *Cadm1^{flx/flx}* mice ($n = 7$) and control littermates (+/?) ($n = 6$) after delivery of AAV-Cre to the hippocampus. (g) Stereotaxic delivery of a mCherry-expressing AAV to paraventricular nucleus (PVH) (red) revealed PVH efferent projections to eGFP-positive POMC neurons (green) in the Arc region of the hypothalamus. Dotted white circle outlines the cell body of an eGFP-POMC-positive cell, used for three-dimensional (3D) reconstruction. (h) Surface rendering of Amira 3D reconstruction of an eGFP-POMC-positive cell body receiving afferent input from the PVH. Cell is represented in red; the synaptic input is color coded, with the cold to warm colors spreading from 0- to 250-nm distance between axonal varicosities and the soma (see color-coded horizontal bar for the distance definition). (i) Histograms show the number of anterograde AAV-mCherry-labeled PVH axonal varicosities found within 250 nm of the POMC-positive cell body. (j) Double immunostaining of *Cadm1* and mCherry or synaptophysin (Syn) revealed that PVH regions provide *Cadm1*-positive efferent projections to the ARC region of hypothalamus. POMC-eGFP transgenic mice received an AAV-mCherry injection to the PVH, and were subsequently immunostained for *Cadm1* (green) and mCherry (red) or synaptophysin (magenta). (k) Representative coronal brain section of *Cadm1* floxed mice after stereotaxic injection of AAV8-CaMKIIa-mCherry-Cre to hypothalamic neurons in the PVH region to drive Cre expression to excitatory neurons in this region. Section shows mCherry expression and staining for vasopressin (green) and nuclei counterstained with DAPI (blue). (l) Confocal imaging of mCherry (red) and vasopressin (green). (m) Body weight curves of *Cadm1^{flx/flx}* mice ($n = 9$) and control littermates (+/?) ($n = 11$) after delivery of AAV-Cre to the hypothalamus. (n) Quantification of energy expenditure adjusted to LBM in 10-week-old *Cadm1^{flx/flx}* mice ($n = 10$) and control littermates (+/?) ($n = 9$) after delivery of AAV-Cre to the hypothalamus. (o) Quantification of energy expenditure adjusted to locomotor activity in 10-week-old *Cadm1^{flx/flx}* mice ($n = 10$) and control littermates (+/?) ($n = 9$) after delivery of AAV-Cre to the hypothalamus. (p) Quantification of food intake measured in *Cadm1^{flx/flx}* mice ($n = 10$) and control littermates (+/?) ($n = 9$) after delivery of AAV-Cre to the hypothalamus. All results in c and m are presented as mean \pm s.e.m. * $P < 0.05$, ** $P < 0.01$. Boxplots show median, lower and upper quartiles (box), and minimum and maximum (whiskers). Statistical analyses are described in the Online Methods and **Supplementary Table 3**.

mCherry, which allows visualization of Cre expression in the dentate gyrus and, to a lesser extent, in the CA3 region of the hippocampus. Approximately 15 d after delivery of the AAV, *Cadm1^{flox/flox}* mice exhibited lower body weight than control mice (Fig. 5c and Supplementary Figs. 8a). Similar to previous *Cadm1* loss-of-function models, the energy expenditure rate was observed to be elevated after targeting *Cadm1* in the hippocampus, and we confirmed this by ANCOVA after plotting against lean body mass and locomotor activity (Fig. 5d,e and Supplementary Fig. 8b). These data directly demonstrate a crucial role for *Cadm1* expressed in excitatory hippocampal neurons in the regulation of body weight and energy expenditure that is independent of an effect on feeding behavior (Fig. 5f).

We executed a similar strategy in the hypothalamus to delineate the contribution of *Cadm1* to the regulation of body weight in this brain region. We first performed tracing experiments to identify the origins of axonal projections to POMC neurons in the ARC (Supplementary Fig. 8c). Stereotactic delivery of a mCherry-expressing AAV to the paraventricular nucleus of the hypothalamus (PVH) region identified axonal inputs to POMC neurons expressing *Cadm1* (Fig. 5g–j and Supplementary Fig. 10). We then directly eliminated hypothalamic *Cadm1* expression by injection of AAV-Cre into the PVH and the ventromedial nucleus of the hypothalamus of *Cadm1^{flox/flox}* mice (Fig. 5k,l and Supplementary Fig. 8d). Similar to *Cadm1* deletion in the hippocampus, lower body weight and increased energy expenditure were observed ~15 d post-injection in *Cadm1^{flox/flox}* mice compared with controls (Fig. 5m–o and Supplementary Fig. 8e,f). Neither insulin sensitivity nor food intake were altered, indicating that these neuronal regions may be distinct with respect to *Cadm1* function in energy homeostasis (Fig. 5p and Supplementary Fig. 8g). Despite the fact that our tracing analysis did not identify a significant number of hippocampal inputs to POMC neurons in the arcuate nucleus, we did observe hippocampal inputs to the PVH in the hypothalamus (Supplementary Fig. 8h). Tracing analysis also identified axonal tracts originating from the hypothalamus to the dentate gyrus of the hippocampus, suggesting that a closed-loop circuit exists between these *Cadm1*-expressing regions and is involved in energy homeostasis (Supplementary Fig. 8i). In addition, *Cadm1*-positive afferent inputs originating from the habenular nuclei, an important site for regulating voluntary locomotor activity and motivational behavior, were observed on POMC-neurons (Supplementary Fig. 8j–m)²⁷. Given the fact that the medial habenula is functionally connected to the hippocampus via strong efferent projections from septal nuclei²⁸, habenular input to POMC-neurons provides an important bridge between the hippocampus and hypothalamus, indicating that *Cadm1* function in energy homeostasis extends to circuits beyond the ARC.

To determine the contribution of *Cadm1* in energy homeostasis in more distinct hypothalamic populations, we conditionally deleted its expression using established Cre-expressing mouse lines. The specific deletion of *Cadm1* using transgenic *Pomc*-, *Agrp*- and *Sim1*-Cre lines (which express Cre recombinase under the control of the respective promoters in neurons of the ARC or PVH) resulted in no substantial changes in metabolic parameters, including insulin sensitivity, and, in the case of POMC neurons, may reflect the low abundance of *Cadm1* in these specific cell types^{29–31} (Supplementary Fig. 9a–c). *Cadm1* was deleted in *Lepr*-Cre cells (*Lepr*-Cre, *Cadm1^{flox/flox}*) and, in spite of broader expression beyond the hypothalamus, the *Cadm1*-deficient mice in the steady state did not exhibit any phenotypic changes (Supplementary Fig. 9d–g)³². However, crossing this line into the *Lep^{ob/ob}* background (*ob/Lepr*-Cre, *Cadm1^{flox/flox}*) resulted in increased random-fed and fasted blood glucose levels, as well as increased random plasma insulin levels (Supplementary Fig. 9h,i). *ob/Lepr*-Cre, *Cadm1^{flox/flox}* mice consistently showed higher glucose

levels in all tolerance tests, indicating an exacerbation of insulin resistance compared with *Lep^{ob/ob}* controls (Supplementary Fig. 9j–l). Body composition, pancreatic beta-cell mass, energy expenditure rate, locomotor activity and food intake were all indistinguishable between *ob/Lepr*-Cre, *Cadm1^{flox/flox}* and *Lep^{ob/ob}* littermates (Supplementary Fig. 9m–o and Supplementary Table 2). These results demonstrate that the role of *Cadm1* in *Slc32a1*-Cre and *Lepr*-Cre cells is distinct from its function in *Slc17a6*-Cre cells with respect to the maintenance of insulin sensitivity, energy expenditure and glucose homeostasis, and that the function of *Cadm1* is dependent on a diverse set of neurons distributed throughout the brain beyond the traditional neuronal circuits controlling energy expenditure and body weight in the hypothalamus (Supplementary Fig. 10).

DISCUSSION

The precise mechanisms causing obesity remain unknown. It is clear that neuronal pathways regulating energy homeostasis and signaling are key contributors and genome-wide association studies have successfully identified genes that are essential to understanding fundamental aspects of our metabolism^{33,34}. Our results illustrate how increased expression of *Cadm1* in the brain is relevant to weight gain and that reducing its expression in both the hippocampus and hypothalamus can trigger a negative energy balance. The expression of both *Cadm1* and *Cadm2* in several neuronal circuits may indicate that the maintenance of our body weight is intertwined with motor control and coordination, motivational and learning behavior, spatial navigation, cognition and memory. This is further supported by several studies showing that *Cadm1* contributes to synaptic plasticity and the excitatory and inhibitory balance of specific networks^{20,21}. Spatially modulated cells (that is, place cells, border cells and grid cells) in hippocampal-entorhinal circuits contribute to the formation of environment-specific memory maps during spatial orientation and may constitute key circuits in the regulation of energy homeostasis^{35,36}. Future investigations will need to determine how the brain is capable of integrating these neuronal circuits together with our physiology and whether targeting *Cadm1* in specific regions is a viable therapeutic strategy for reversing obesity in humans³⁷.

METHODS

Methods, including statements of data availability and any associated accession codes and references, are available in the online version of the paper.

Note: Any Supplementary Information and Source Data files are available in the online version of the paper.

ACKNOWLEDGMENTS

The authors would like to thank M. Gruhn and the Biozentrum Imaging Facility, University of Cologne, for access to Amira Software, and N. Zampieri, A. Plested, T. Breiderhoff, D. Matthäus, I. Park, C. Teng, T. Klüssendorf, H. Wessels, T. Willnow and M. Gotthardt for helpful discussions and assistance in the conduct of this work. This work was funded by the Helmholtz Gemeinschaft, the Helmholtz Metabolic Dysfunction Consortium, the Helmholtz Alliance ICEMED (Project 1210251 to T.N.), the European Research Council (ERC-2010-StG-260744 to M.N.P., ERC-2015-CoG-682422 to J.F.A.P., ERC-2011-StG-280565 to J.S., and ERC-2013-StG-336607 to M.T.), the US National Institutes of Health (R01-DK-111178, 1P01-AG-051459 and 1R56-AG-052986 to T.L.H.) the Swiss National Science Foundation Professorship (PP00P3_144886 to M.T.), the Deutsche Forschungsgemeinschaft (FOR-2143-Interneuron to J.F.A.P., Exc-257-NeuroCure to J.F.A.P. and V.H., and SFB958/A01 to V.H., and DFG B11292/4-2 and DFG IRTG2251 to A.L.B.), the Federal Ministry of Education and Research (BMBF, Germany) (Project eMed:symAtrial (01ZX1408D to M.H.), the European Foundation for the Study of Diabetes (EFSd, Germany), the Thyssen Foundation, and the Kay Kendall Leukemia Foundation (KKLF Fellowship to L.v.d.W.). AAV reagents were provided by the UNC Vector Core facility and used with permission by K. Deisseroth (Stanford University).

AUTHOR CONTRIBUTIONS

T.R. and M.N.P. conceived the study. T.R., X.Y., N.L.K., M.-C.K., K.S.-B., L.F., V.T., D.P., G.K., S.B., L.V., K.S., C.-X.Y., S.C.S., S.G.T., A.S.C., M.M., J.S., A.H., L.v.d.W., A.L.B., T.N., J.F.A.P., T.L.H., M.H.T., M.H., M.T., V.H. and M.N.P. designed and performed the experiments with help from all of the authors. V.H. and M.N.P. wrote the manuscript.

COMPETING FINANCIAL INTERESTS

The authors declare no competing financial interests.

Reprints and permissions information is available online at <http://www.nature.com/reprints/index.html>. Publisher's note: Springer Nature remains neutral with regard to jurisdictional claims in published maps and institutional affiliations.

- Finkelstein, E.A. *et al.* The lifetime medical cost burden of overweight and obesity: implications for obesity prevention. *Obesity (Silver Spring)* **16**, 1843–1848 (2008).
- McCarthy, M.I. & Zeggini, E. Genome-wide association studies in type 2 diabetes. *Curr. Diab. Rep.* **9**, 164–171 (2009).
- Grant, S.F.A. *et al.* Variant of transcription factor 7-like 2 (TCF7L2) gene confers risk of type 2 diabetes. *Nat. Genet.* **38**, 320–323 (2006).
- Frayling, T.M. Genome-wide association studies provide new insights into type 2 diabetes aetiology. *Nat. Rev. Genet.* **8**, 657–662 (2007).
- Willer, C.J. *et al.* Six new loci associated with body mass index highlight a neuronal influence on body weight regulation. *Nat. Genet.* **41**, 25–34 (2009).
- Speliotes, E.K. *et al.* Association analyses of 249,796 individuals reveal 18 new loci associated with body mass index. *Nat. Genet.* **42**, 937–948 (2010).
- Locke, A.E. *et al.* Genetic studies of body mass index yield new insights for obesity biology. *Nature* **518**, 197–206 (2015).
- Biederer, T. *et al.* SynCAM, a synaptic adhesion molecule that drives synapse assembly. *Science* **297**, 1525–1531 (2002).
- Fogel, A.I. *et al.* SynCAMs organize synapses through heterophilic adhesion. *J. Neurosci.* **27**, 12516–12530 (2007).
- Fogel, A.I. *et al.* N-glycosylation at the SynCAM (synaptic cell adhesion molecule) immunoglobulin interface modulates synaptic adhesion. *J. Biol. Chem.* **285**, 34864–34874 (2010).
- GTEX Consortium. Human genomics. The Genotype-Tissue Expression (GTEx) pilot analysis: multitissue gene regulation in humans. *Science* **348**, 648–660 (2015).
- Biederer, T. Bioinformatic characterization of the SynCAM family of immunoglobulin-like domain-containing adhesion molecules. *Genomics* **87**, 139–150 (2006).
- Badman, M.K., Kennedy, A.R., Adams, A.C., Pissios, P. & Maratos-Flier, E. A very low carbohydrate ketogenic diet improves glucose tolerance in ob/ob mice independently of weight loss. *Am. J. Physiol. Endocrinol. Metab.* **297**, E1197–E1204 (2009).
- Elias, C.F. *et al.* Leptin differentially regulates NPY and POMC neurons projecting to the lateral hypothalamic area. *Neuron* **23**, 775–786 (1999).
- Brüning, J.C. *et al.* Role of brain insulin receptor in control of body weight and reproduction. *Science* **289**, 2122–2125 (2000).
- Ahima, R.S., Bjorbaek, C., Osei, S. & Flier, J.S. Regulation of neuronal and glial proteins by leptin: implications for brain development. *Endocrinology* **140**, 2755–2762 (1999).
- Tschöp, M.H. *et al.* A guide to analysis of mouse energy metabolism. *Nat. Methods* **9**, 57–63 (2011).
- Huo, L. *et al.* Leptin-dependent control of glucose balance and locomotor activity by POMC neurons. *Cell Metab.* **9**, 537–547 (2009).
- Vong, L. *et al.* Leptin action on GABAergic neurons prevents obesity and reduces inhibitory tone to POMC neurons. *Neuron* **71**, 142–154 (2011).
- Robbins, E.M. *et al.* SynCAM 1 adhesion dynamically regulates synapse number and impacts plasticity and learning. *Neuron* **68**, 894–906 (2010).
- Park, K.A. *et al.* Excitatory synaptic drive and feedforward inhibition in the hippocampal CA3 circuit are regulated by SynCAM 1. *J. Neurosci.* **36**, 7464–7475 (2016).
- Kerchner, G.A. & Nicoll, R.A. Silent synapses and the emergence of a postsynaptic mechanism for LTP. *Nat. Rev. Neurosci.* **9**, 813–825 (2008).
- Turrigiano, G. Too many cooks? Intrinsic and synaptic homeostatic mechanisms in cortical circuit refinement. *Annu. Rev. Neurosci.* **34**, 89–103 (2011).
- Perez de Arce, K. *et al.* Topographic mapping of the synaptic cleft into adhesive nanodomains. *Neuron* **88**, 1165–1172 (2015).
- van Praag, H., Kempermann, G. & Gage, F.H. Running increases cell proliferation and neurogenesis in the adult mouse dentate gyrus. *Nat. Neurosci.* **2**, 266–270 (1999).
- van Praag, H., Christie, B.R., Sejnowski, T.J. & Gage, F.H. Running enhances neurogenesis, learning, and long-term potentiation in mice. *Proc. Natl. Acad. Sci. USA* **96**, 13427–13431 (1999).
- Hsu, Y.-W.A. *et al.* Role of the dorsal medial habenula in the regulation of voluntary activity, motor function, hedonic state, and primary reinforcement. *J. Neurosci.* **34**, 11366–11384 (2014).
- Bianco, I.H. & Wilson, S.W. The habenular nuclei: a conserved asymmetric relay station in the vertebrate brain. *Philos Trans R Soc Lond B Biol Sci* **364**, 1005–1020 (2009).
- Balthasar, N. *et al.* Leptin receptor signaling in POMC neurons is required for normal body weight homeostasis. *Neuron* **42**, 983–991 (2004).
- Balthasar, N. *et al.* Divergence of melanocortin pathways in the control of food intake and energy expenditure. *Cell* **123**, 493–505 (2005).
- Hill, J.W. *et al.* Direct insulin and leptin action on pro-opiomelanocortin neurons is required for normal glucose homeostasis and fertility. *Cell Metab.* **11**, 286–297 (2010).
- DeFalco, J. *et al.* Virus-assisted mapping of neural inputs to a feeding center in the hypothalamus. *Science* **291**, 2608–2613 (2001).
- Billings, L.K. & Florez, J.C. The genetics of type 2 diabetes: what have we learned from GWAS? *Ann. NY Acad. Sci.* **1212**, 59–77 (2010).
- Loos, R.J.F. & Yeo, G.S.H. The bigger picture of FTO: the first GWAS-identified obesity gene. *Nat. Rev. Endocrinol.* **10**, 51–61 (2014).
- Moser, M.-B., Rowland, D.C. & Moser, E.I. Place cells, grid cells and memory. *Cold Spring Harb. Perspect. Biol.* **7**, a021808 (2015).
- Hartley, T., Lever, C., Burgess, N. & O'Keefe, J. Space in the brain: how the hippocampal formation supports spatial cognition. *Phil. Trans. R. Soc. Lond. B* **369**, 20120510 (2013).
- Zeltser, L.M., Seeley, R.J. & Tschöp, M.H. Synaptic plasticity in neuronal circuits regulating energy balance. *Nat. Neurosci.* **15**, 1336–1342 (2012).

ONLINE METHODS

Animals. Mice were housed in groups of 3–5 animals and maintained on a 12-h light/dark cycle with ad libitum access to regular chow food, high fat diet (containing 60% kcal fat, cat. no. E15741-347, ssniff Spezialdiäten GmbH), or ketogenic diet (cat. no. E15149-30, ssniff Spezialdiäten GmbH) in accordance with the Landesamt für Gesundheit und Soziales (LAGeSo). All experimental procedures were approved under protocols G 0357/10, G 0204/14, O 0405/09 and T 0436/08. Cadm1KO mice³⁸ were characterized after backcrossing for four generations to C57BL/6 and then crossed to *Lep^{ob/ob}* and POMC-eGFP expressing mice (Jackson Labs). Cadm2KO mice were generated by the trans-NIH Knockout Mouse Project (KOMP) and obtained from the KOMP Repository (<http://www.komp.org>). Mice expressing *Slc17a6-Cre*, *Slc32a1-Cre*, *Lepr-Cre*, *AgRP-Cre*, *Sim1-Cre* and *Pomc-Cre* were purchased (Jackson Labs) and directly crossed to *Cadm1* floxed mice that were previously crossed to C57BL/6 (Jackson Labs) for four generations. To generate Tg-Cadm1 mice, full-length *Cadm1* cDNA flanked by seven repeats of the doxycycline-responsive element was inserted into pTRE-Tight vector (Clontech) before microinjection. Positive founders were crossed to *Slc17a6-Cre* and ROSA26-rtTA mice (Jackson Labs). All experiments implemented Cre-expressing mice as controls to account for potential metabolic abnormalities³⁹. Results were consistent in both genders however data from female mice is not shown.

Analytic procedures. Quantification of metabolic parameters. Guinea pig anti-insulin (Dako A0564, 1:500) and rabbit anti-glucagon (Millipore AB932, 1:500) antibodies for immunofluorescence were used on paraffin-embedded pancreata fixed in 4% paraformaldehyde (PFA). Plasma glucose levels were obtained with the One Touch glucometer (Bayer). Plasma and total pancreatic insulin measurements were measured by radioimmunoassay or ELISA as described (Millipore, Crystal Chem)⁴⁰. Plasma leptin was measured by ELISA (Peprotech) and adiponectin by radioimmunoassay (Millipore).

Antibodies for western blot analysis. The following primary antibodies were used for western blotting at 1:1,000 dilution: Cadm1 (MBL CM004-3), Cadm2 (Sigma SAB4501053), β -actin (Sigma A1978), GAPDH (Abcam ab8245), γ -tubulin (Sigma T6557) and PSD95 (NeuroMab UCDavis 075 028). Variance in the banding patterns of Cadm proteins in different panels may result from variation in acrylamide percentage or levels of protein glycosylation. Image densitometry of 16-bit TIF images for all western blots was performed using ImageJ. All full-length blots are presented in **Supplementary Figures 11–15**.

Primary cell cultures. Primary neurons were derived from hippocampi of mice at postnatal day 2 and dissected in cold HBSS (Invitrogen), followed by digestion with papain. After centrifugation, tissue pellet was resuspended in Neurobasal (Invitrogen) supplemented with B27 (Invitrogen) and Glutamax (Invitrogen) for plating. Hippocampal cells were cultured in 24-well dishes with 12-mm coverslips (5,000 cells per coverslip) coated with poly-D-lysine and laminin and immunohistochemistry was performed as described previously⁴¹. After post-fixation in 4% PFA, sections were blocked with 10% BSA/PBS, then incubated with primary antibody overnight at 4 °C, followed by the fluorochrome-conjugated secondary antibodies for 1 h. Fluorescence was imaged under a confocal microscope (Zeiss LSM700). Digital images were analyzed with Fiji/ImageJ.

Mouse phenotyping. All phenotyping analysis was performed in a 'blinded' manner; genotypes were unknown to the investigator during the experimentation and age of animals is stated in figure legends. All genotypes were present during all experiments and randomization was implemented to the extent that all animals were identified by number before analysis.

Body composition and energy expenditure analysis. Body composition analysis was measured using Minispec Model LF90 II (6.5 mHz) (Bruker Instruments). VO₂, VCO₂, food intake and locomotor activity were measured using the PhenoMaster System (TSE) and energy expenditure was analyzed as previously described using ANCOVA¹⁷. Animals were placed into individual cages with weight sensors quantifying ad libitum access to food. VO₂ and VCO₂ level were measured for 1 min at 9-min intervals for 4 consecutive days and locomotor activity was measured continuously by breaks of light beams. The first 24 h of measuring time was excluded from the analysis to allow for acclimation to the new cage environment. Measurement of energy expenditure was normalized to lean body mass as previously described⁴².

Tolerance tests. Glucose and pyruvate tolerance tests were performed following an overnight fast (16 h) and injected intraperitoneally with either glucose (2 g/kg body weight) or pyruvate (2 g/kg body weight in saline) as described⁴⁰. Insulin tolerance tests were performed after same day fast (6 h) by injecting insulin (Sigma) intraperitoneally (0.75 U/kg body weight). Murine leptin (Peprotech) (0.75 μ g/g body weight) was injected intraperitoneally twice daily (09:00 and 19:00) for 3 d. Body weight and food intake were measured daily at 08:30.

In vivo clamp studies. Clamp studies were performed as described⁴³. Plasma [³H] glucose was measured by scintillation counting of ZnSO₄/Ba(OH)₂ deproteinized serum, dried to remove ³H₂O. Calculations were obtained as follows: Basal and insulin-stimulated whole body glucose turnover rates = ($[(3\text{-}^3\text{H})\text{ glucose infusion (in dpm)}]/(\text{plasma glucose specific activity (dpm per mg)})$) at the end of the basal period and during the final 30 min of the clamp, respectively. Hepatic glucose production = (rate of total glucose appearance) – (glucose infusion rate). Plasma concentration of ³H₂O = ³H counts [wet] – [dry]. Whole body glycolysis was defined by the rate of increase in plasma ³H₂O concentration by linear regression of measurements between 90–140 min. Whole body glycogen synthesis = (whole body glucose uptake) – (whole body glycolysis). Tissue ¹⁴C-2-deoxyglucose-6-phosphate content was measured following sample homogenizing, and the supernatant's ¹⁴C-2-deoxyglucose-6-phosphate was separated from 2-deoxyglucose by ion-exchange column.

In vivo cold exposure analysis. Cold challenge was performed as described previously⁴⁴. Briefly, 12-week-old mice were kept at 6 °C for 14 consecutive days in a light and humidity-controlled climate chamber (TSE Systems) and fed chow diet *ad libitum*.

Tracing analysis and AAV injections. Stereotaxic injections were performed on 5–8-week old mice and all data incorporated into the analysis was obtained from animals that were examined histologically for mCherry expression in the appropriate nuclei. For POMC-eGFP/*Slc17a6-Cre* mice, rAAV2/EF1a-DIO-hChR2(H134R)-mCherry (UNC Vector Core, titer 6.6×10^{12} vg/ml) was unilaterally injected into the dentate gyrus (DG) of the hippocampus, habenular nuclei (Hb) and paraventricular nucleus of the hypothalamus (PVH) respectively ($n = 4$); rAAV5/EF1a-DIO-hChR2(H134R)-mCherry (UNC Vector Core, titer 5×10^{12} vg/ml) was unilaterally injected into the habenular nuclei (Hb) ($n = 4$). Briefly, the mouse was anesthetized with ketamine (120 mg/kg), Xylazine (10 mg/kg) and an i.c. injection of analgesic Metamizol (200 mg/kg). Next, an incision on the head skin was performed and animals were placed in a stereotaxic frame (Angle Two, Leica) while maintained at a temperature of 37.5 °C with a heating pad during the whole operation. A small craniotomy was performed over the DG with coordinates: 1.8 mm posterior, 1.3 mm lateral to Bregma; Hb: 1.6 mm posterior, 0.36 mm lateral to Bregma; PVH: 0.7 mm posterior, 0.24 mm lateral to Bregma. A glass injection pipette with a ~10–20- μ m diameter tip containing the AAV solution was then inserted to the following depths: 1.8 mm (for DG), 2.7 mm (for Hb) and 4.8 mm (for PVH). Using an oil piston (MO-10; Narishige) connected to this injection glass pipette 0.1–0.4 μ l of virus was injected at a rate of 50–100 nl/min. The injection pipette stayed in place for about 10 min to allow the pressure to equilibrate after the injection and then removed. Post-injection, the incision site was stitched with suture thread and the mice recovered on a heating pad at 37.5 °C with access to water with Metamizol (0.2 mg/ml) for 24 h. *Cadm1^{fllox/fllox}* mice and littermate controls were stereotaxically injected with rAAV8/CamKII-mCherry-Cre resulting in expression of the mCherry-Cre fusion protein (UNC Vector Core). Mice were anesthetized with Ketamine HCl/Xylazine HCl (50/5 mg/kg, intraperitoneally) and restrained in a Kopf stereotaxic frame (David Kopf Instruments). Small holes with the size of the injection needle were drilled into the skull, and injections were done bilaterally with 1 μ l of vector per brain region. The rAAV8/CamKII-mCherry-Cre was administered (0.5 μ l for the PVH and 1 μ l for the dentate gyrus, titer: 4.7×10^{12} virus genome/ml) into the dentate gyrus (coordinates: –1.7 mm from bregma, ± 1.5 mm lateral, –2.2 mm from the surface of the skull) and PVH (coordinates: –0.82 mm from bregma, ± 0.5 mm lateral, –5.0 mm from the surface of the skull). Animals/samples were excluded if proper injection of the AAVs could not be validated by reporter expression and immunohistochemistry.

Immunohistochemistry and image analysis. Mice were transcardially perfused with 50 ml saline solution (0.85% NaCl, 0.025% KCl, 0.02% NaHCO₃, pH 6.9, 0.01% heparin, body temperature) followed by 50 ml cold (7–15 °C) freshly

depolymerized 4% PFA in 0.1 M PBS, pH 7.4. Brains were post-fixed overnight in the same fixative and placed in a mixture of 20% glycerol and 2% dimethyl sulfoxide in 0.4 M PBS for 24 h for cryoprotection. Frozen horizontal or coronal sections (40 μm) were collected in 0.1 M PBS. The following antibodies were used for immunohistochemistry: Cadm1 (MBL CM004-3, 1:500), Cadm2 (Sysy 243203, 1:500), POMC (Phoenix H-029-30, 1:500), Synaptophysin (Sysy 100011, 1:500), Vasopressin (Millipore AB1565, 1:1,000), NeuN (Abcam ab177487, 1:500; Millipore MAB377, 1:100), MAP2 (Sysy 188004, 1:1,000), VGAT (Sysy 131004, 1:500), mCherry (Abcam ab125096, 1:500), GFP (Thermo Fisher A11120, 1:500) and VGLUT2 (Sysy 135402, 1:500) were used. Sections were washed 3 \times in PBS (3 \times 15 min each) followed by washing several times in PBS containing 0.3% Triton-X-100 (9 \times 20 min each). Sections were pre-incubated with PBS containing 5% NGS and 0.3% Triton X-100 for 1 h, and subsequently incubated with primary antibody at 4 $^{\circ}\text{C}$ for 48 h. Then, sections were washed nine times for 20 min each in 0.3% Triton X-100 in 0.1 M PBS, and incubated with Alexa-conjugated secondary antibodies (1:400) for 12 h using standard techniques. Finally, sections were mounted on gelatin-coated glass slides and coverslipped in Immu-Mount. Immunofluorescent images were acquired using a Leica SP5 confocal microscope, equipped with a 488-nm argon laser, a 561-nm DPSS laser and a 633 red Helium Neon laser. To detect fluorescence emission sections were scanned at a resolution of 1,024 \times 1,024 pixels with 8-bit sampling in sequential scanning frame-by-frame mode. Cadm1 expression levels were quantified in ImageJ by measuring the mean gray value of fluorescence intensity within the ROI using 20 \times Plan-Apochromat objective. For high-resolution 3D analysis, samples were scanned using Plan-Apochromat 63 \times /1.32 Oil DIC objective at a resolution of 1,024 \times 1,024 pixels with 8-bit sampling in sequential scanning frame-by-frame mode. Single optical sections were acquired using identical acquisition settings, with the pinhole of 1 Airy Unit. Stacks of 8–29 optical sections yielded voxel dimensions between 100 and 400 nm for the X, Y and Z planes. 3D reconstructions were generated with Amira Software (FEI Visualization Sciences). First, the cell body of the POMC-positive neurons was reconstructed using Amira surface editor. Synaptic input was defined by the reconstruction of AAV-mCherry positive varicosities in the same image using Isosurface module. The likely synaptic contact was defined by color-coding the surface of AAV-mCherry positive varicosities found within 250 nm from POMC-positive cell body. Subsequently, the surface of '250-nm-distant' AAV-mCherry-positive varicosities was mapped onto POMC-positive cell body using the 'map distance' tool.

Analysis of Cadm1 and Vglut2 fluorescent profiles. Overlap of fluorescent intensity profiles of Cadm1 and Vglut2 was measured using the line scan function of ImageJ on an x - y plane of a single optical section. Subsequently line profiles were analyzed using custom-developed Python script. In detail, the percentage of overlap between Cadm1 and Vglut2 was analyzed according to the following algorithm:

$$100 * \left(1 - \frac{\sum_{i=1}^n |y_{follow_i} - y_{lead_i}| * y_{lead_i}^2}{\sum_{i=1}^n y_{lead_i}^3} \right).$$

First, all fluorescent values were normalized by scaling them from 0–1,000 and the penalty values were calculated by taking the absolute value of the difference between the *lead* curve (Vglut2) and the *follow* curve (Cadm1) ($|y_{follow_i} - y_{lead_i}|$). The 'Events' of fluorescent puncta were defined by the presence of high y -values of the lead curve. To account for the overlap of two curves in these areas the penalty values were multiplied with the square of the lead y -value, giving the term: $|y_{follow_i} - y_{lead_i}| * y_{lead_i}^2$. Next, a measurement for the differences between the two curves was generated by taking the sum of all penalty values (sum1): $\sum_{i=1}^n |y_{follow_i} - y_{lead_i}| * y_{lead_i}^2$. The penalty was restricted to the interval 0–100% by dividing the actual penalty value by the maximum possible penalty (sum2): $\sum_{i=1}^n y_{lead_i}^3$.

Electron microscopy analysis. 8-week old mice were anesthetized and transcardially perfused with 4% formaldehyde and 2.5% glutaraldehyde in PBS. Brains were isolated and post-fixed in the same solution overnight at 4 $^{\circ}\text{C}$ after rinsing in PBS, and then embedded into 5% agar and sliced coronally (200- μm sections). Vibratome slices containing hippocampi were post-fixed in 1% OsO₄ and 1.5% potassium hexacyanoferrat, followed by dehydration in a methanol gradient and propylene oxide, and flat embedded in epoxy resin. After polymerization the CA1

pyramidal cell layer and adjacent stratum radiatum were trimmed and ultrathin sectioned. Sections were collected on coated slotted grids and analyzed using a Zeiss 900 transmission electron microscope. Synaptic density was determined by the dissector method⁴⁵. Neuropil images with an area of $\approx 190 \mu\text{m}^2$ from adjacent sections with defined thickness were aligned, a dissector grid was superimposed onto the images and the appearance of the postsynaptic density was used as a 'counting cap'. At least 20 dissectors were analyzed per animal and density of synaptic profiles was estimated in two dimensions by counting number of profiles in 160 neuropil fields.

Quantification of excitatory and inhibitory synapses was performed as previously described⁴⁶. Mice were perfused using Somogyi-Takagi fixative; the brain was removed and a tissue block containing the hypothalamus was sectioned. EGFP (derived from the POMC-eGFP transgene) was stained using an anti-GFP antibody for signal amplification (Molecular Probes A-11120, 1:500) and ABC Elite Kit (Vector Labs). Sections were subsequently osmicated, dehydrated and ultrathin sections obtained using a microtome. Images were acquired using a Tecna 12 Biotwin (FEI Company) electron microscope. Non-symmetric (excitatory) and symmetric (inhibitory) synapse numbers on POMC neurons were quantified in a double-blinded fashion using the dissector technique. Synapses were only quantified if a clear identification of pre- and postsynaptic membranes was possible and synaptic vesicles in the presynaptic bouton were visible. Synapses without a clear non-symmetric or symmetric specialization were excluded from the analysis.

Electrophysiological analysis. For EPSCs and IPSCs, the entire brain from 3-week-old animals was removed and immediately submerged in ice-cold, carbogen-saturated (95% O₂ / 5% CO₂) aCSF (in mM: 2.5KCl, 126 NaCl, 1.3 MgCl₂, 2.0 CaCl₂, 1.2 KH₂PO₄, 21.4 NaHCO₃, 10 glucose). Coronal sections (300 μm) were cut with a Leica VT1000S Vibratome and then incubated in oxygenated aCSF at 22–24 $^{\circ}\text{C}$ for at least 1 h before recording. Whole-cell voltage-clamp recordings from POMC-eGFP neurons (identified with the POMC-eGFP transgene)⁴⁷ were performed using a Multiclamp 700B amplifier (Molecular Devices) and filtered with an eight-pole Bessel filter at 6 kHz. Both voltage and current signals were sampled at 50 kHz using an Axon 1440A interface device (Molecular Devices) and the data were acquired using Clampex 10.2 software (Molecular Devices). Electrodes were pulled using a micropipette puller (Sutter Instruments) from thick-walled borosilicate glass GC150F capillaries (Harvard Apparatus) to a resistance of $\sim 3 \text{ M}\Omega$. Series resistance compensation ranged from 50 to 70% and recordings were discarded if the series resistance exceeded 10 M Ω . Electrodes were filled with an internal solution of composition (in mM) 140 CsCl, 4 NaCl, 0.5 CaCl₂, 10 HEPES, 5 EGTA, 2 Mg-ATP, QX-314-Br 3, pH 7.3 with CsOH, and osmolarity of 290 mOsm. Cells were visualized using an infrared differential interference contrast (DIC) optics equipped with equipped ORCA-R2 camera (Hamamatsu) mounted on a Slicescope (Scientifica) with a 40 \times water-immersion objective. Neurons were voltage clamped at -70 mV . To record IPSCs, the aCSF composition included 3 mM kynurenic acid (Sigma) to block excitatory glutamatergic activity. EPSCs were recorded in presence of Picrotoxin (Tocris) 100 μM in order to block both GABA and Gly evoked currents. Both experimental conditions included TTX 0.5 μM (Tocris) to isolate miniature events. Events were excluded from the analysis if their amplitude was less than 3 s.d. of the baseline noise and if there were overlapping events within 50 ms (for IPSCs) or 10 ms (for EPSCs). All miniature events were automatically detected with Clampfit 10, followed by manual inspection of single events. For frequency distributions a minimum of 200 events were analyzed.

For MPP-DG recordings, 6–8-week old WT and Cadm1^{Slc17a6} mice were used for acute hippocampal field electrophysiology. Mice were decapitated after cervical dislocation and the brain extracted into ice cold dissection 'cutting' solution containing (in mM): 2.5 KCl, 1.25 NaH₂PO₄, 24 NaHCO₃, 1.5 MgSO₄, 2 CaCl₂, 25 glucose, 250 sucrose. 350 μm sagittal brain slices prepared from both hemispheres were transferred to a resting chamber containing solution in which 250 mM sucrose was replaced with 120 mM NaCl (pH = 7.35–7.4) and incubated to recover before recordings. Recordings performed at 22–24 $^{\circ}\text{C}$ in the submerged chamber, supplied with continuously bubbled solution with an exchange of 3–5 ml per min. Stimulating (1–1.5 M Ω) and recording (1.5–2.5 M Ω) electrodes filled with solution were placed in inner part of molecular layer of DG and medial perforant path (MPP) to DG field excitatory postsynaptic potentials (fEPSPs) were recorded. Basal stimulation of 0.2 ms electrical pulses was delivered at every

30 s for at least 10 min to monitor stable baseline recordings. Only the responses which show paired pulse depression were considered as MPP and were studied further to evaluate synaptic transmission and plasticity. The stimulus response curves made as a measure of basal synaptic transmission in which stimulation intensity was increased from 10 to 100 μ A, reaching maximal responses at around 60–70 μ A for both genotypes. For long-term potentiation (LTP) and long-term depression (LTD) recordings, baseline stimulation was set to elicit 50% of maximal fEPSP (30–40 μ A) and GABAergic antagonist picrotoxin (100 μ M) was applied to recording solution at least 30 min before the LTP and LTD induction. Stimulation intensity was doubled during LTP, LTD induction using stimulation intensities at which maximal fEPSPs were detected (60–70 μ A). 5 \times HFS were delivered every 30 s each HFS containing 100 pulses at 100 Hz for LTP induction and LFS containing 900 pulses at 1 Hz stimulation was used for LTD induction. LTP and LTD was calculated as the percentage increase of fEPSP slope 50–60 min after application of induction protocol as compared to the initial –10 to 0 min of baseline. The data were recorded at a sampling rate of 10 kHz, low-pass filtered at 3 kHz and analyzed using PatchMaster software and EPC9 amplifier (Heka Electronics).

eQTL analysis. We have downloaded currently unpublished eQTL data from the GTEx consortium analysis version 6, including results from ten distinct brain regions⁴⁸. We specifically queried the data for association tests that were performed for genes *CADM1* and *CADM2* against SNPs rs12286929 and rs13078807. Adjustment for multiple hypothesis testing using the method of Benjamini and Hochberg showed that all associations were significant (FDR \leq 15%)⁴⁹. Boxplots were obtained through the GTEx portal.

Statistical analysis. All results are expressed as mean \pm s.e.m. Comparisons between data sets with two groups were evaluated using an unpaired Student's *t* test. One-way and two-way repeated-measures ANOVA analysis has been performed using GraphPad Prism Software Version 6.07 for comparisons of three or more groups. Post hoc statistics were performed using Sidak's multiple

comparison test. A *P* value of less than or equal to 0.05 was considered statistically significant. The presented data met the assumptions of the statistical tests used. Normality and equal variances were tested using GraphPad Prism software. No statistical methods were used to pre-determine sample sizes, but our sample sizes are similar to those reported in previous publications^{17,29–31,40,43}.

A **Supplementary Methods Checklist** is available.

Data availability. All primary data supporting the findings of this study are available on reasonable request.

38. van der Weyden, L. *et al.* Loss of TSLC1 causes male infertility due to a defect at the spermatid stage of spermatogenesis. *Mol. Cell. Biol.* **26**, 3595–3609 (2006).
39. Harno, E., Cottrell, E.C. & White, A. Metabolic pitfalls of CNS Cre-based technology. *Cell Metab.* **18**, 21–28 (2013).
40. Tattikota, S.G. *et al.* Argonaute2 mediates compensatory expansion of the pancreatic β cell. *Cell Metab.* **19**, 122–134 (2014).
41. Glynn, M.W. & McAllister, A.K. Immunocytochemistry and quantification of protein colocalization in cultured neurons. *Nat. Protoc.* **1**, 1287–1296 (2006).
42. Butler, A.A. & Kozak, L.P. A recurring problem with the analysis of energy expenditure in genetic models expressing lean and obese phenotypes. *Diabetes* **59**, 323–329 (2010).
43. Birkenfeld, A.L. *et al.* Deletion of the mammalian INDY homolog mimics aspects of dietary restriction and protects against adiposity and insulin resistance in mice. *Cell Metab.* **14**, 184–195 (2011).
44. Chevalier, C. *et al.* Gut microbiota orchestrates energy homeostasis during cold. *Cell* **163**, 1360–1374 (2015).
45. Jeffrey, M. *et al.* Synapse loss associated with abnormal PrP precedes neuronal degeneration in the scrapie-infected murine hippocampus. *Neuropathol. Appl. Neurobiol.* **26**, 41–54 (2000).
46. Pinto, S. *et al.* Rapid rewiring of arcuate nucleus feeding circuits by leptin. *Science* **304**, 110–115 (2004).
47. Cowley, M.A. *et al.* Leptin activates anorexigenic POMC neurons through a neural network in the arcuate nucleus. *Nature* **411**, 480–484 (2001).
48. GTEx Consortium. The Genotype-Tissue Expression (GTEx) project. *Nat. Genet.* **45**, 580–585 (2013).
49. Benjamini, Y. & Hochberg, Y. Controlling the false discovery rate: a practical and powerful approach to multiple testing. *J. R. Stat. Soc. Ser. B Methodol.* **57**, 289–300 (1995).